JOINT EUROPEAN TORUS

JET–P(91)53

C. Gormezano, M. Brusati, A. Ekedahl, P. Froissard, J. Jacquinot,
F. Rimini and JET Team

Synergistic Effects Between Lower Hybrid and Fast Magnetosonic Waves in JET

Synergistic Effects Between Lower Hybrid and Fast Magnetosonic Waves in JET

C. Gormezano, M. Brusati, A. Ekedahl, P. Froissard, J. Jacquinot,
F. Rimini and JET Team*

JET-Joint Undertaking, Culham Science Centre, OX14 3DB, Abingdon, UK

** See Appendix 1*

Preprint of a paper to be submitted for publication in Proceedings of
IAEA Technical Committee on Fast Wave Current Drive in Reactors

J5/GG/TSC744/jh
9.10.91

SYNERGISTIC EFFECTS BETWEEN LOWER HYBRID AND FAST MAGNETOSONIC WAVES IN JET

C GORMEZANO, M BRUSATI, A EKEDAHL, P FROISSARD
J JACQUINOT, F RIMINI

JET JOINT UNDERTAKING

Synergism: The condition in which the result of the combined action of two or more agents is greater than the sum of their separate individual actions (from the Greek synergos: working together) Chambers Science and Technology dictionary- Cambridge.

Abstract

Combined Lower Hybrid Current Drive and Ion Cyclotron Resonance Heating experiments have been carried out in JET, starting in 1990 with the prototype LH system. Non-inductive currents up to 1.5 MA have been produced in ICRF heated plasmas with volume averaged electron temperature of 2.2 keV. The main "signature" of synergy is the large increase in the photon temperature of the hard X-ray emission, representative of the fast electron distribution, which has been observed during combined LH plus ICRH heating. Deposition profiles of direct electron heating have been obtained by means of LH power modulation experiments. In presence of ICRH, they exhibit an enhanced power transfer in the plasma core which cannot be accounted for by the launched LH power alone. A possible explanation is the electron damping of the fast wave on fast electron tail via Transit Time Magnetic Pumping leading to the observed heating and current drive efficiency.

Plan

The paper will be divided along the following lines:

- Possible synergistic effects between Lower Hybrid Current Drive and Ion Cyclotron Resonance Heating.
- LHCD and ICRH systems and plasma range of parameters.
- Fast electron bremmsthralung diagnostic.
- Acceleration of LHCD induced fast electrons in ICRH heated plasmas.
- Domain of observation of "synergistic" effect.
- Central electron temperature increase.
- Current drive efficiency.

POSSIBLE SYNERGISTICS EFFECTS

LH Current Drive efficiency is inversely proportional to $N_{\parallel}$. Therefore, an improved current drive efficiency is expected if $N_{\parallel}$ downshifts during wave propagation.

Change of LH wave propagation properties and absorption can be anticipated when the temperature and density profiles vary significantly as it is the case in ICRH heated plasmas. According to ray tracing studies made at JET /1/, there are no significant changes in the $N_{\parallel}$ spectrum, at least during the first pass. Propagation in the plasma centre might depend upon plasma edge conditions. Multiple pass ray tracing usually leads to a $N_{\parallel}$ upshift but not to a $N_{\parallel}$ downshift.

A more likely possible synergy mechanism is direct damping of ICRH waves on the fast electron population induced by LHCD as predicated for instance in the calculations for TTMP damping /2/. The ICRH power launched via a fast wave can be damped /3/:

- by cyclotron resonance on a minority population, which leads to the build-up of a fast ion tail resulting in electron and ion heating;
- by mode conversion which might result in electron heating;
- by transit time magnetic pumping which result in the build-up of a fast electron tail.

In the latter case, the force acting on the electrons is proportional to $\mu\nabla\tilde{B}$,where μ is the electron magnetic moment and $\tilde{B}$ the RF magnetic field. It is to be noted that other effects such as torsional Alfven wave damping are not yet taken into account by theory /4/. RF wave damping is proportional to the density of fast electrons /2/ /5/. An asymmetric parallel fast electron tail is present in the plasma as a result of LHCD; the ICRH wave can further accelerates this population thus producing an extra amount of current drive without the need to phase the ICRF wave.

Coupling of the ICRF wave to the electrons via mode conversion is a possible scheme, especially with low $k_{\parallel}$ for which the damping is low. The damping of the resulting waves on the fast electron population is not yet assessed.

EXPERIMENTAL CONDITIONS FOR COMBINED LHCD AND ICRF

LHCD experiments have been performed on JET with a prototype system consisting of 16 multijunctions splitting into 128 narrow waveguides facing the plasma /6/. Each horizontal row of multijunctions consists of 16 waveguides. Build in phase shifters give a $\pi/2$ phasing between adjacent waveguides of given multijunction. The resulting wave spectrum is centred at $N_{\parallel} = 1.8$ (in resonance with 100 keV electrons) with a 70% directivity. The peak $N_{\parallel}$ value can be varied from 1.4 to 2.4 by varying the phase between klystrons.

The launcher is powered by 8 klystrons capable of launching into the torus up to 3.2 MW for 10 sec. or 3.8 MW for 20 sec. The complete LHCD system, to be installed in 1993, will consist of 24 klystrons feeding 384 waveguides via 48 multijunctions. The LHCD data presented in this paper have been obtained with power ranging from 1.2 to 2.4 MW with klystrons phases tuned to obtain the central value of $N_{\parallel} = 1.8$.

The ICRH system on JET is well known /7/. It has been operated in monopole and dipole configurations at frequencies ranging from 28 to 52 MHz. The plasma parameters were the following:

- B_{ϕ} from 2 to 3.4 T
- I_p from 1 to 3 MA
- n_{eo} from 2 to 3.5 10^{19} m^{-3}

As shown in figure 1, there is a large variation of the target electron temperature profile from Teo : 3 - 11.5 keV. As a result, large variations in the fast electron profiles were observed as it will be discussed later.

THE FAST ELECTRON BREMMSTHRALUNG DIAGNOSTIC

The FEB diagnostic/8/ is a multichord detection system designed to detect hard X-ray emission in the range 100 keV upwards. It comprises a vertical and a horizontal camera of 9 and 10 detectors respectively (CsI Ti crystal) viewing the plasma poloidal cross section through an inconel window of respectively 1.5 mm thick (vertical port) and 4 mm thick (horizontal port). Photon emission is recorded for 4 equal energy intervals in the range 100 to 300 keV for each detector line of sight.

A schematic of the FEB cameras is given in figure 2. Further to the FEB, the forward X-ray emission above 3 keV is monitored by a Ge detector located at the end of a narrowly collimated tangential line of sight forming an angle of 22° with the magnetic axis.

An example of the photon spectrum in the forward direction is shown in figure 3 for an LH only plasma pulse. The corresponding perpendicular spectra as measured by the vertical and the horizontal FEB cameras are given in figure 4 and 5 for the same plasma pulse, showing an acceptable agreement.

Unfortunately, when the Ge detector is used for combined ICRH and LHCD experiments, the signal level is so high that the corresponding data are not reliable. An X-ray attenuator has to be installed. Data from the vertical FEB camera are also affected during combined operation by the large X-ray signal through the thin inconel port.

Therefore, all data which will subsequently be presented in this paper will be from the horizontal FEB camera, profiles being obtained by means of Abel inversion on the magnetic flux surfaces. Depending upon the plasmas conditions, a large variety of fast electron profiles have been achieved:

- very peaked profiles as in figure 6 for a low density, high magnetic field case.

- rather hollow profiles as in figure 7 for a higher density. Fast electron peakedness increases with increasing magnetic field. This effect can be explained by a better penetration of the wave at higher magnetic field as predicted from accessibility conditions.

ACCELERATION OF LHCD INDUCED FAST ELECTRONS IN ICRH HEATED PLASMAS

In some plasma conditions described later, it is possible to observe:

- an acceleration of the fast electrons;

- an increased current drive.

An example of electron acceleration is given in figure 8. The photon spectrum with LH only extends up to about 300 keV, i.e. above the interacting range which extends up to about 180 keV. The additional acceleration can be explained by the well known "synergistic" effect with the remaining E field from the inductive drive. During combined ICRH LHCD operation, the photon spectrum extends up 450 keV. It is to be noted that the loop voltage was zero for the latter conditions. The synergy with the E field drops and the electron acceleration can only be explained by :

- a downshift of the $N_{\parallel}$ spectrum;

- a damping of the ICRH wave on the fast electron population.

A comparison of the photon spectrum is given in figure 9 for:

- a zero loop voltage plasma achieved with LH only (0.4 MA);

- a non-zero loop voltage plasma achieved with LH only (1.5 MA);

- a zero loop voltage plasma achieved with LH + ICRH (1.5 MA) with similar densities ($n_{eo} = 2.5\ 10^{19} m^{-3}$).

A very large increase in the number of photons in the 300 keV range is observed for the combined heating. We have tried to simulate the observed photon temperature by assuming a given set of parameters for the fast electron distribution, following ref. /9/. In addition, we have assumed a cut-off energy for the electrons:

Parallel temperature	350 keV	900 keV	900 keV
Perpendicular temperature	100 keV	300 keV	300 keV
Electron cut-off energy	400 keV	400 keV	800 keV
Resulting calculated perpendicular photon temperature	63 keV	84 keV	140 keV

Such a simulation is not exhaustive but shows that a significant acceleration of the fast electron population, up to energies close to the 1 MeV has to be assumed in order to simulate the observed photon temperatures.

DOMAIN OF OBSERVATION OF "SYNERGISTICS" EFFECTS

Synergistics effects between LH and ICRH have been observed so far in JET only in a restricted set of conditions leading to a high fast electron density near the plasma centre. This can be achieved by:

- operating at low density;
- using peak electron temperature profiles which occurs:
    a) at high magnetic field;
    b) during "monsters" sawteeth;
    c) for plasmas with high internal inductance.
- operating with the maximum LH power.

Synergistics effects have not so far been observed:

- in discharges with high Z_{eff};
- in high density discharges ($n_{eo} > 3\ 10^{19}\ m^{-3}$);
- when the ICRH system was in dipole configuration;
- when the phases of the LH klystrons were not properly tuned.

The effect of increasing LH power is documented in figure 10 and 11 by comparing two 1.5 MA, 3 T discharge powered respectively with 1.2 MW and a 2.3 MW LH power, with similar ICRF power and similar target plasma parameters. An LH only pulse at 2.3 MW is also shown for comparison. From figure 10, it can be seem that a clear increase of the photon temperature takes place only at high LH power and that the maximum increase occurs where the density of the high energy photons is the highest (from figure 10). The increase of photons on the low energy channel is roughly proportional to the LH power while the high energy channel shows a dramatic increase at about 20 to 30 cm from the magnetic axis.

From FEB data analysis during 100% LH modulation discharges, it can be seen that the background signal, due to high energy gamma rays and neutrons induced by ICRH, can be neglected over the energy range that has been used /8/.

CENTRAL ELECTRON TEMPERATURE INCREASE

The behaviour of the fast electron profiles as inferred from the high energy photon emission profiles, seems to indicate the possibility of current drive slightly off-axis, and therefore possible changes in the local shear with a resulting improvement in the electron confinement. In the 1990 campaign an improved electron heating was observed during combined ICRH and LHCD operation /3/ /10/. The evolution of the central electron temperature versus the total injected power normalised to the central density is shown in figure 12. Low value of P_{tot}/n_e are obtained with a relatively high value of the electron density for which synergy is not observed. High value of P_{tot}/n_e correspond to low density operation with high RF power for which carbon bloom was very often observed. The corresponding rise in Z_{eff} might explain the lack of synergistic effects at high combined power.

CURRENT DRIVE EFFICIENCY

As presented in earlier publications, enhanced non-inductive current drive appears to be associated with the observation of synergistics effects.

The current drive efficiency data base on JET now includes data with full current drive: at 0.4 MA with LH alone and at 1 and 1.5 MA with combined ICRF and LHCD operation, as shown in figure 13. A bootstrap current of 0.3 MA has been estimated for the plasma pulse shown in figure 13. Current drive efficiencies are calculated using the following formula:

$$\eta_{CD} = \bar{n}_e R \frac{I_{NI} - I_{BS}}{P_{CD}}$$

where:

- $\bar{n}_e$ is the line averaged density;
- I_{NI} is the non-inductive current drive estimated from loop voltage drop, taking into account resistive effects and time derivative of plasma inductance;
- I_{BS} is the bootstrap estimated from ref /11/. To be noted that JET experiments conform to the current scaling $I_{BS}/I_P \sim 0.45\ \beta_p$.
- $P_{CD} = P_{LH} + I_{NI} \times V_{loop} + P_{TTMP}$

Current drive efficiencies, assuming that all the power driving the non-inductive current is given by the LH wave, is plotted in figure 14 versus the volume averaged electron temperature. Possible bootstrap current is taken into account. It is to be noted that data obtained with full current drive agrees quite well with data already published where an inductive drive is still present. A "good" agreement is found with a linear scaling law /12/ with the volume averaged electron temperature, up to <Te> of about 1.8 keV.

Synergy leads to a factor 2 increase in efficiency respect to the linear temperature scaling. Unfortunately, the FEB camera data were not available for the data corresponding to <Te> above 2 keV.

Power coupled to the fast electron population is estimated from estimation of the radial electron deposition profile. The bulk electron deposition profile is deduced from the change in the time derivative of the electron temperature as discussed in /13/. The deposition profiles corresponding to conditions with and without observation, of synergistic effects, are given in figure 15. Without synergy, 70% of the launched LH power can be estimated to be coupled to the bulk electron population, while this ratio is up to 125% of the LH power when synergy is observed. It can then be assumed that a significant part of the ICRF power, approximately in the range of 10%, is coupled to the electrons. Theoretical estimates of the damping of the fast wave on the fast electron population induced by LHCD are given in /14/. Damping in the 5 to 10% range can be estimated assuming a 200 keV isotropic fast electron population with a 0.15% concentration of fast electrons.

The data base shown in figure 13 can be corrected by assuming than 10% of the ICRH power contributes to the current drive as shown in figure 16. The current drive efficiency then does not exceed significantly the maximum value which can be estimated from Fisch /15/, assuming that 70% of the power is coupled to the fast electrons and the $N_{\parallel}$ stays at its launched value.

SUMMARY

Combined LHCD and ICRH experiments have been performed in a variety of plasma conditions, including a variation of central electron temperature from 3 to 11 keV. Synergistic effects defined as:

- acceleration of fast electrons up to a few hundreds of keV (at the location where the fast electron population density is highest);
- increased current drive : up to 1.5 MA;
- large current drive efficiency: $\bar{n}$ R I/P up to 0.57 10^{20} m^{-3} (assuming that current drive is only produced by LH);

have been achieved when:

- a large fast electron population is established in the inner half of the plasma;
- the target plasma has peaked electron temperature and density profiles;
- the electron density remains low ($n_{eo} < 2.8\ 10^{19}\ m^{-3}$);
- the LH power exceeds 1.5 MW.

Synergistics effects can be due to:

- a downshift of $N_{||}$, which appears to be an unlikely possibility;

- a direct coupling of the ICRH fast wave:

  a) by direct TTMP or torsional Alfven wave damping;

  b) by mode conversion, which appears also to be unlikely.

An experimental campaign aiming at optimising these effects remains to be done. Radial electron deposition profiles appears to show that about 10% of the ICRF power can be directly coupled to the electron population, indicating that up to 300 kA of the current is driven by the ICRF wave. The possible utilisation of LHCD/ICRF synergy includes:

- an increase LH current drive leading to an improved current profile control;

- production of a reversed magnetic shear configuration which might improve the electron confinement allowing higher electron temperature to be achieved.

- an increase of the TTMP current drive if inwards diffusion of fast electrons is significant in large and hot plasmas.

References

/1/ M Brusati, C Gormezano, S Knowlton, M Lorenz-Gottardi, F Rimini: 8th Topical Conference on RF Power in Plasmas, Irvine (1989).

/2/ D Moreau et al. in Controlled Fusion and Plasma Physcis)Proc. 14th Eur. Conf., Madrid, 1987) Vol. III, 1007.

/3/ J Jacquinot, in Controlled Fusion and Plasma Physics (Proc. 18th Eur. Conf., Berlin 1991) to be published.

/4/ SC Shiu et al., Nuclear Fusion 26 (1986) 1619.

/5/ L Samain, P Becoulet, private communcation.

/6/ C Gormezano et al., Proceedings 12th Symp. on Fusion. Eng., Vol I (Monterey, 1987).

/7/ D Start, these proceedings.

/8/ P Froissard et al., in Proceedings 18th Eur. Conf. Cont. Fusion and Plasma Phys., Berlin (1991) III, 393.

/9/ Von Goeler et al., Rev. Sc. Instr. 1986.

/10/ D Moreau, C Gormezano in Controlled Fusion and Plasma Physcis (Proc. 18th Eur. Conf., Berlin, 1991) to be published.

/11/ C Challis, private communication.

/12/ K Ushigusa, Proceedings Con. Fus. and plasma Heating, 17th EPS Amsterdam, Vol 32, 11 (1990) 853.

/13/ V Bathnagar, these proceedings.

/15/ N Fisch, Phys. Rev. Lett. 41 (1978) 873.
Phys. Fluids 28 (1985) 245.

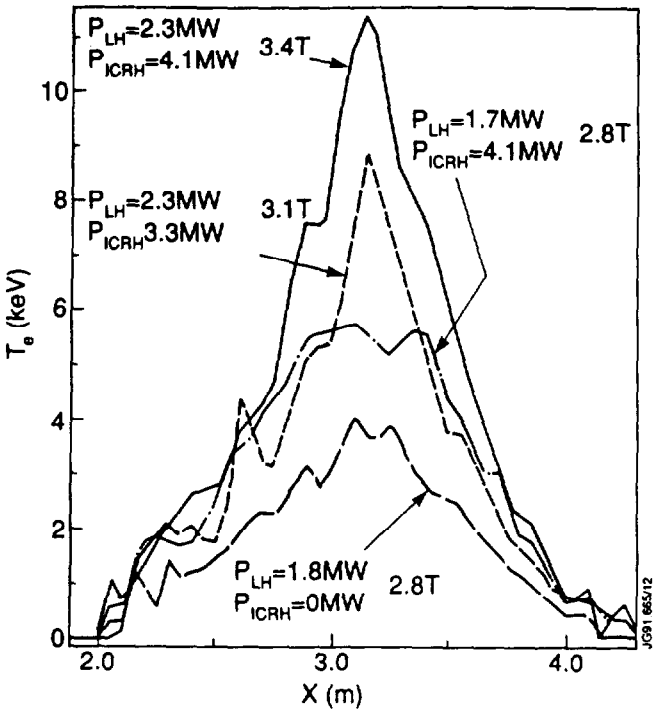

Fig 1: Changes in electron temperature profiles (from Lidar diagnostic)

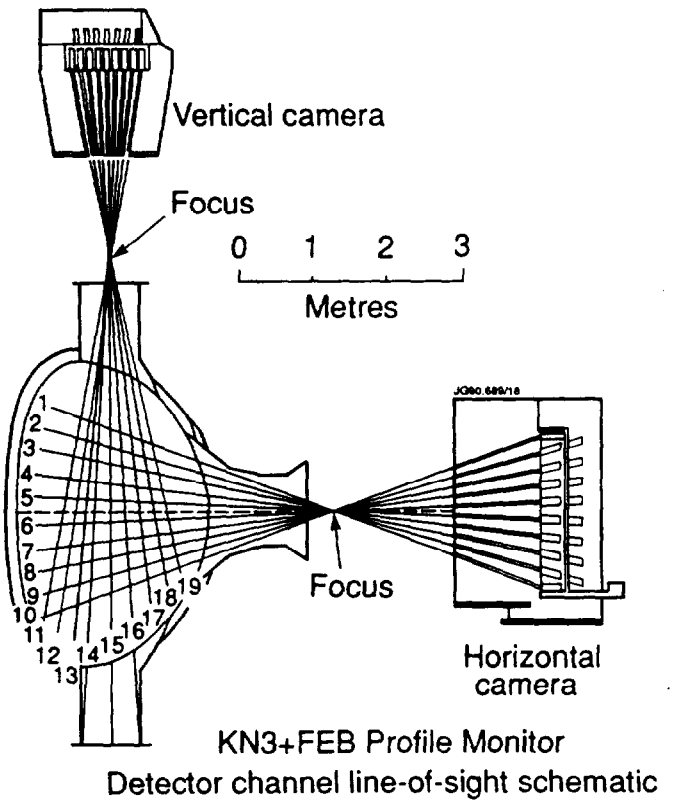

Fig 2: Schematic of the FEB cameras

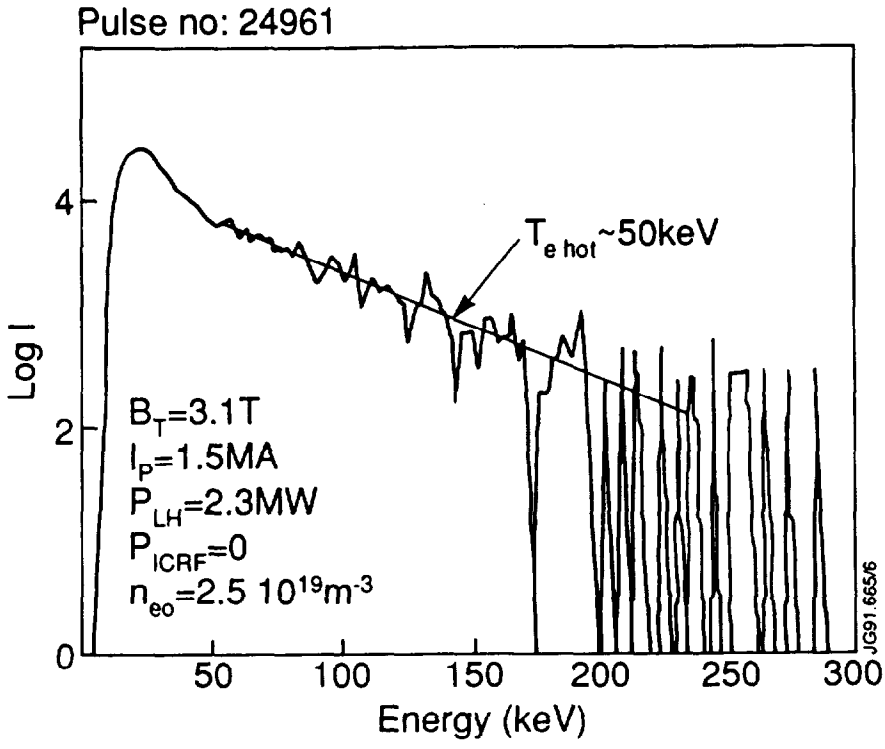

Fig 3: Photon temperature from the forward X-ray emission diagnostic

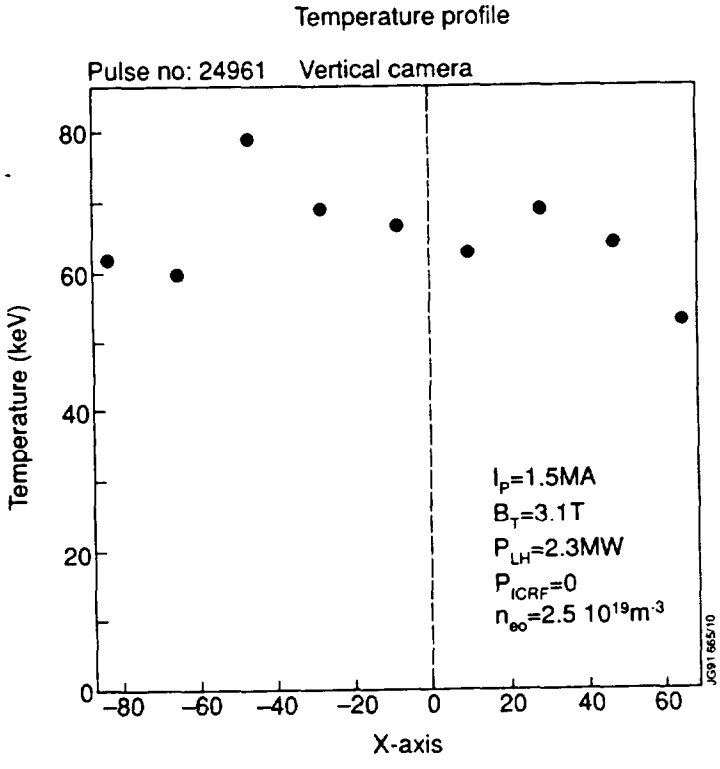

Fig 4: Photon temperature from the vertical FEB camera

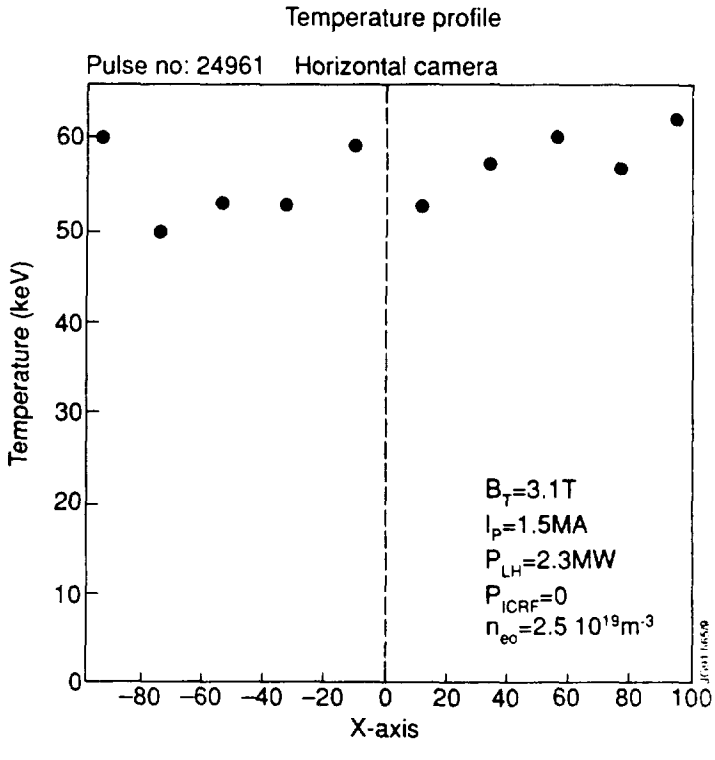

Fig 5: Photon temperature from the horizontal FEB camera

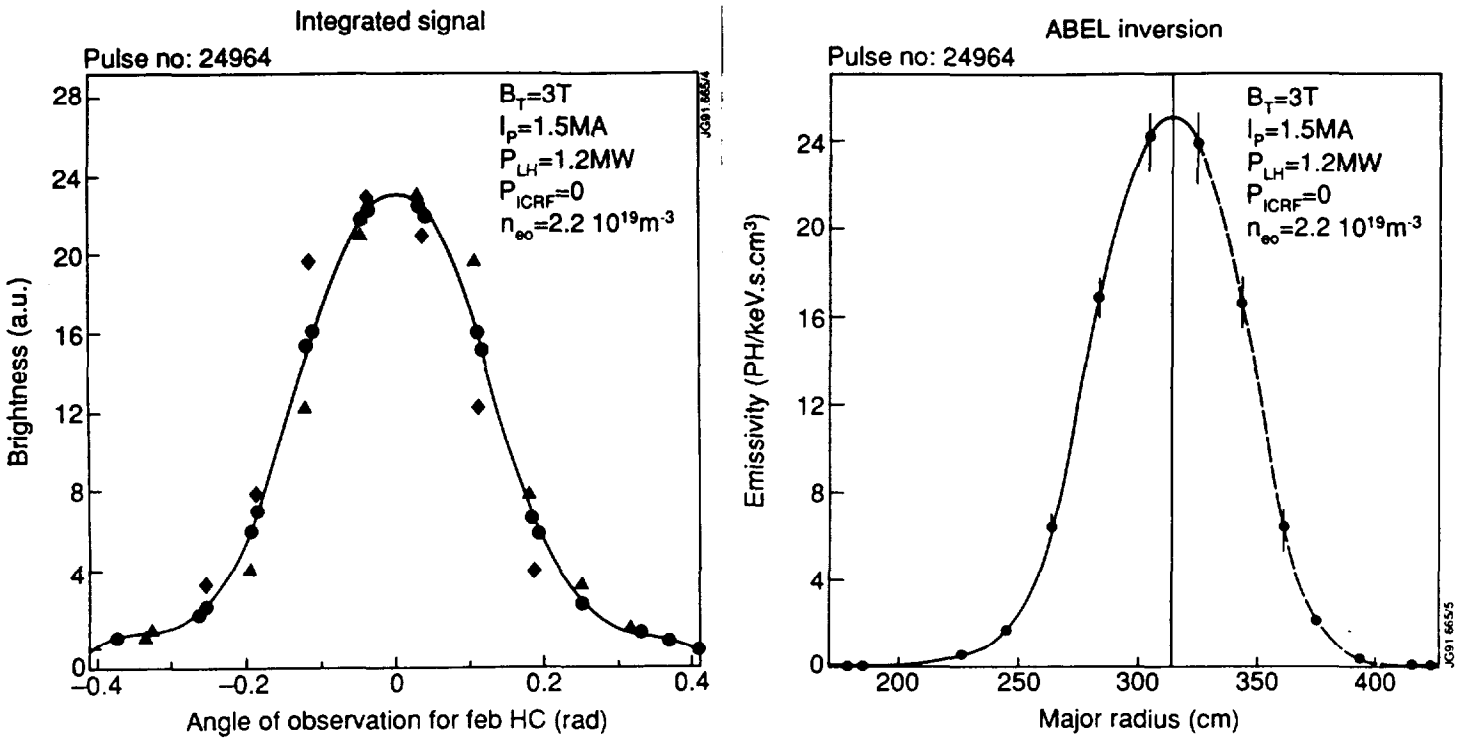

Fig 6: Radial profile of the photon emission from the horizontal FEB camera (100 - 150 keV range)

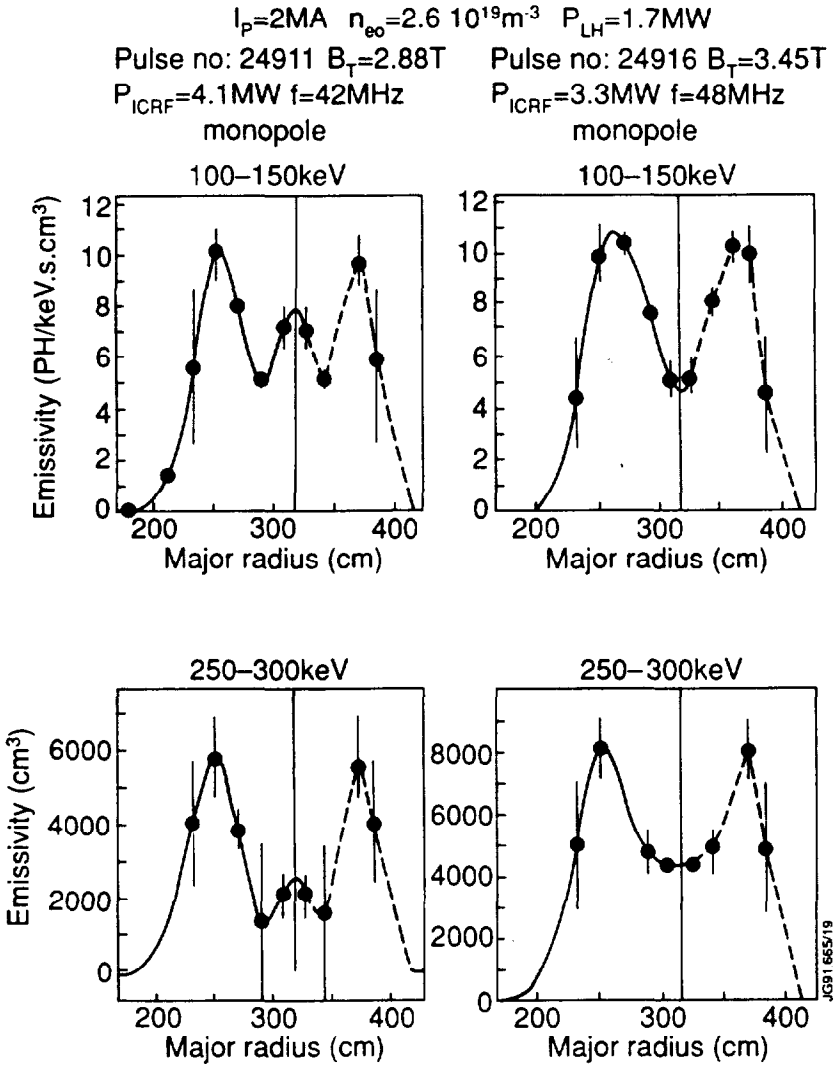

Fig 7: Influence of the toroidal magnetic field on radial profile of the photon emission (from horizontal FEB camera)

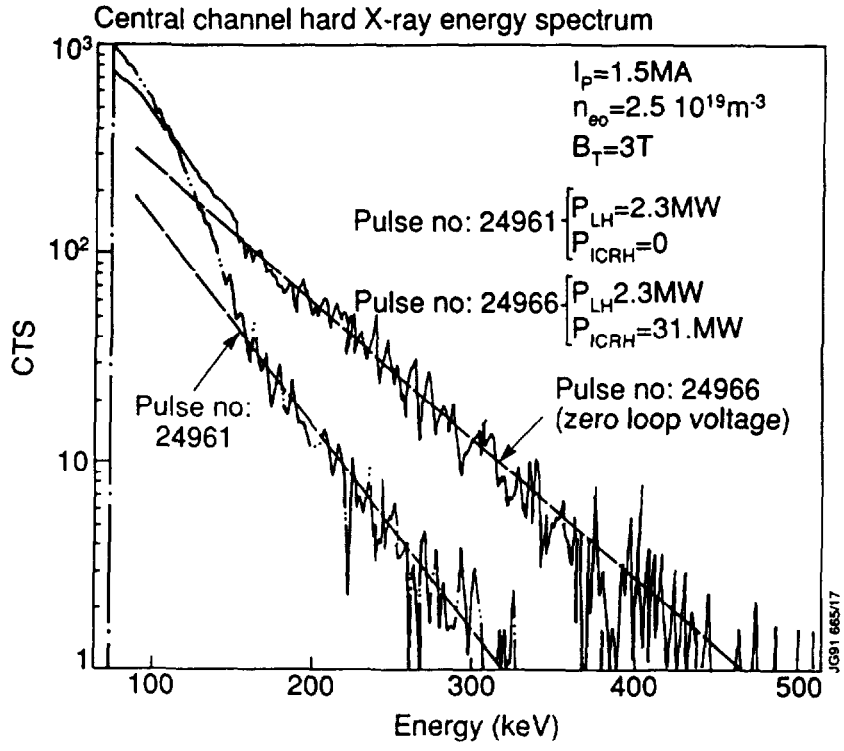

Fig 8: X-ray energy spectra from horizontal FEB camera

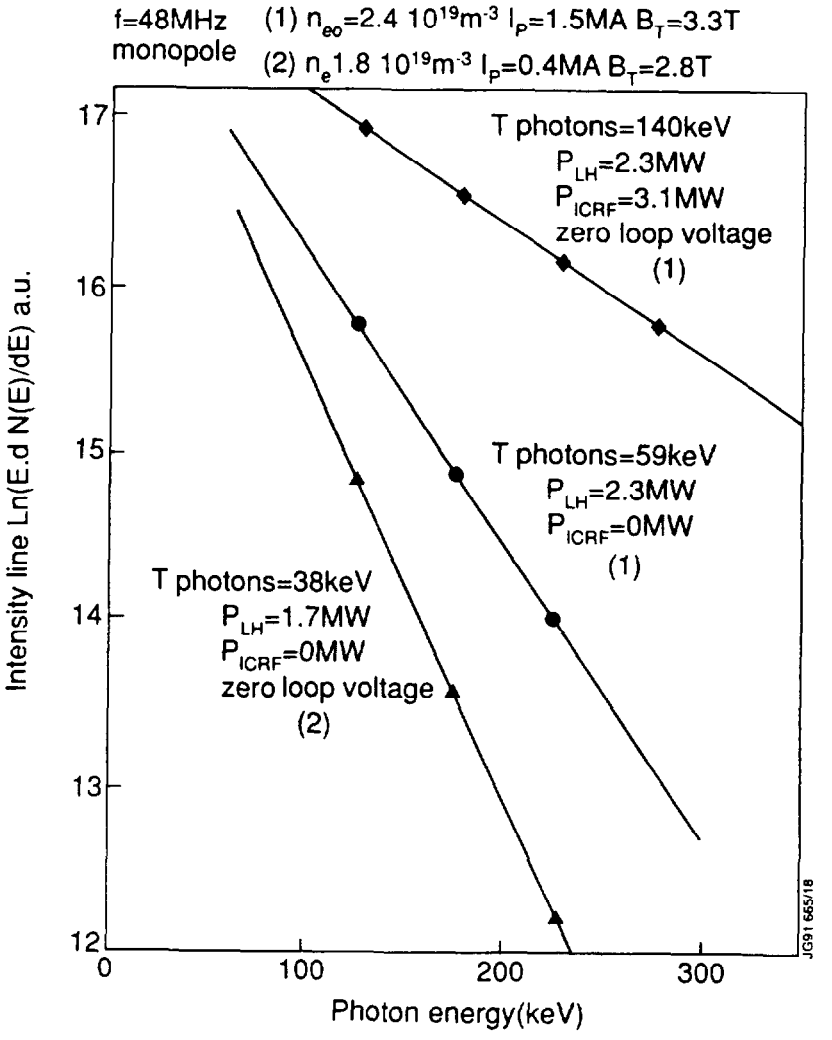

Fig 9 :X-ray energy spectra from horizontal FEB camera (channel 7)

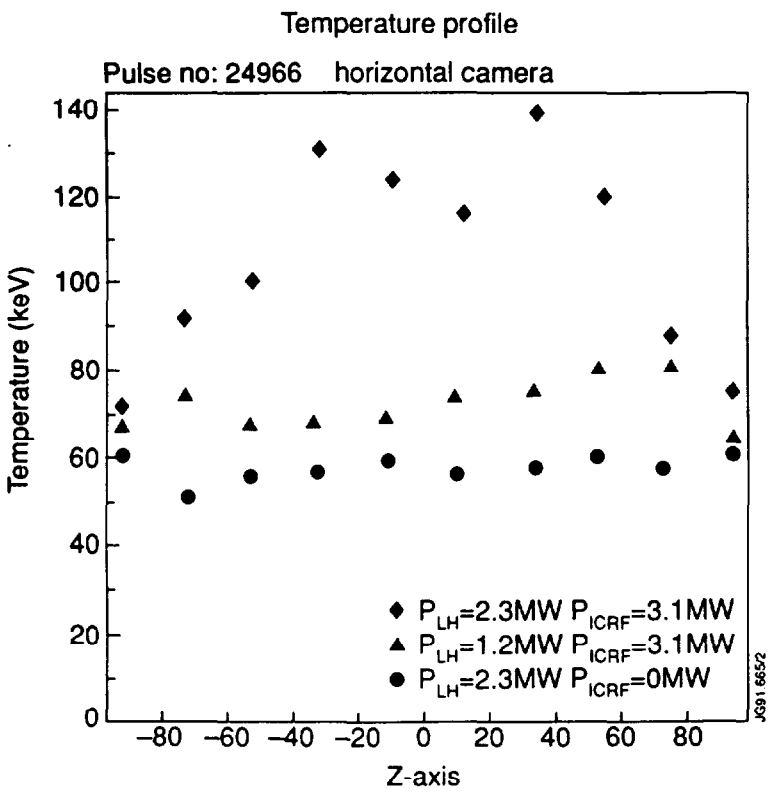

Fig 10: Influence of LH power on the photon temperature profile.

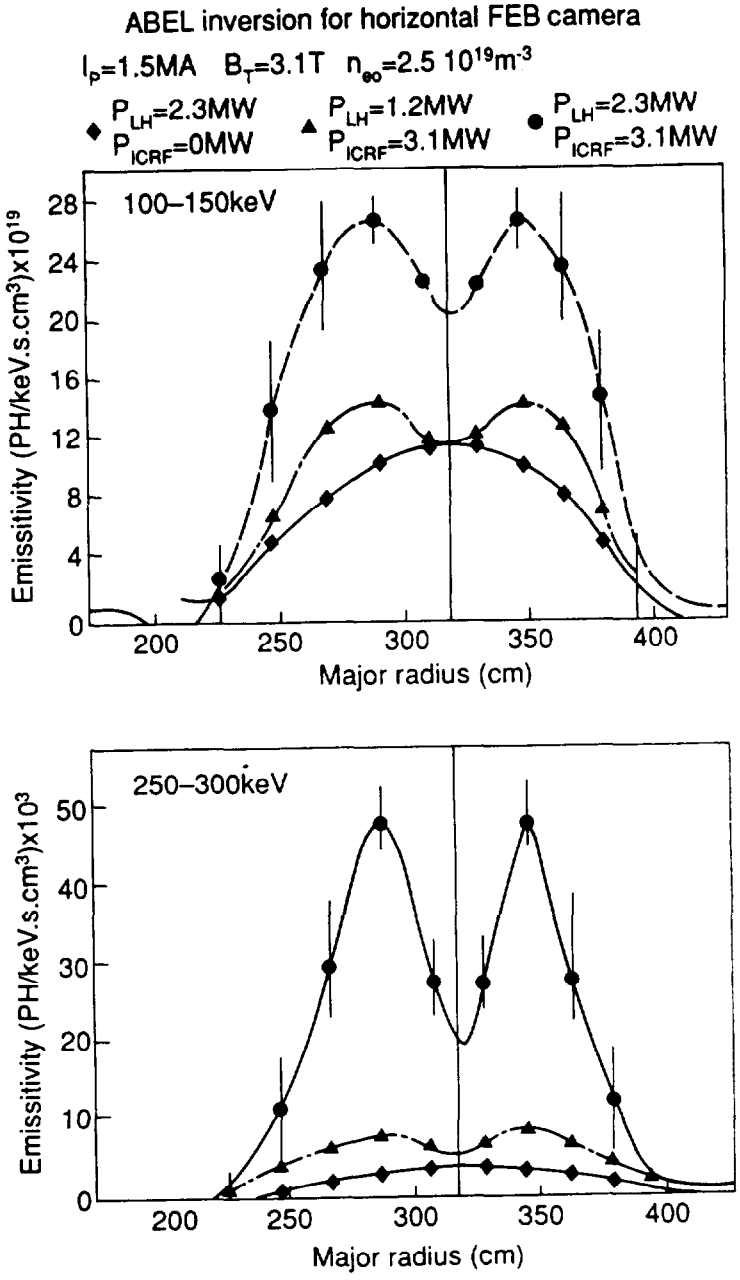

Fig 11: Influence of LH power on the photon radial distribution for two energy range.

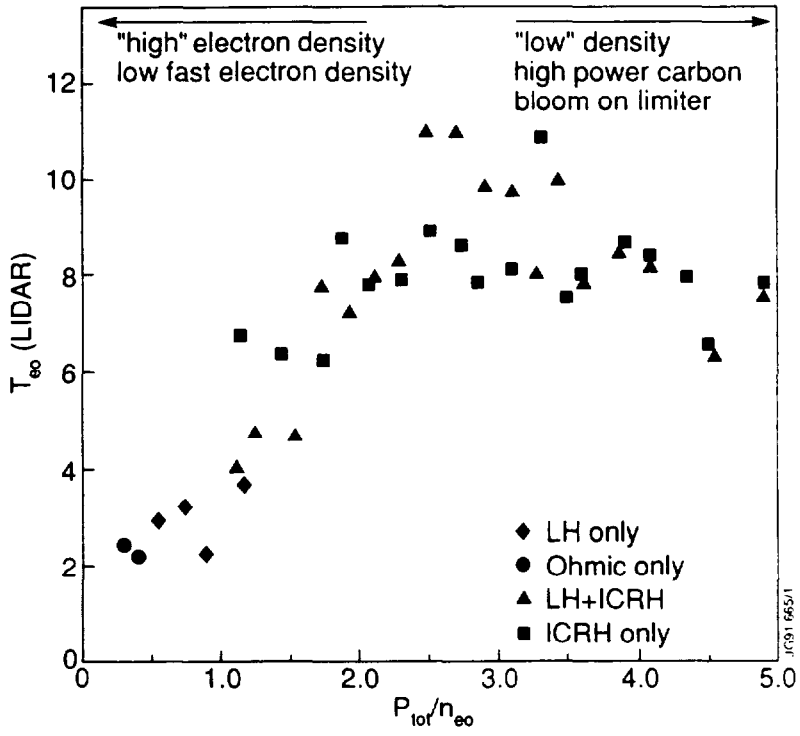

Fig 12: Evolution of the central electron temperature versus total injected power normalised to central density (from Lidar diagnostic)

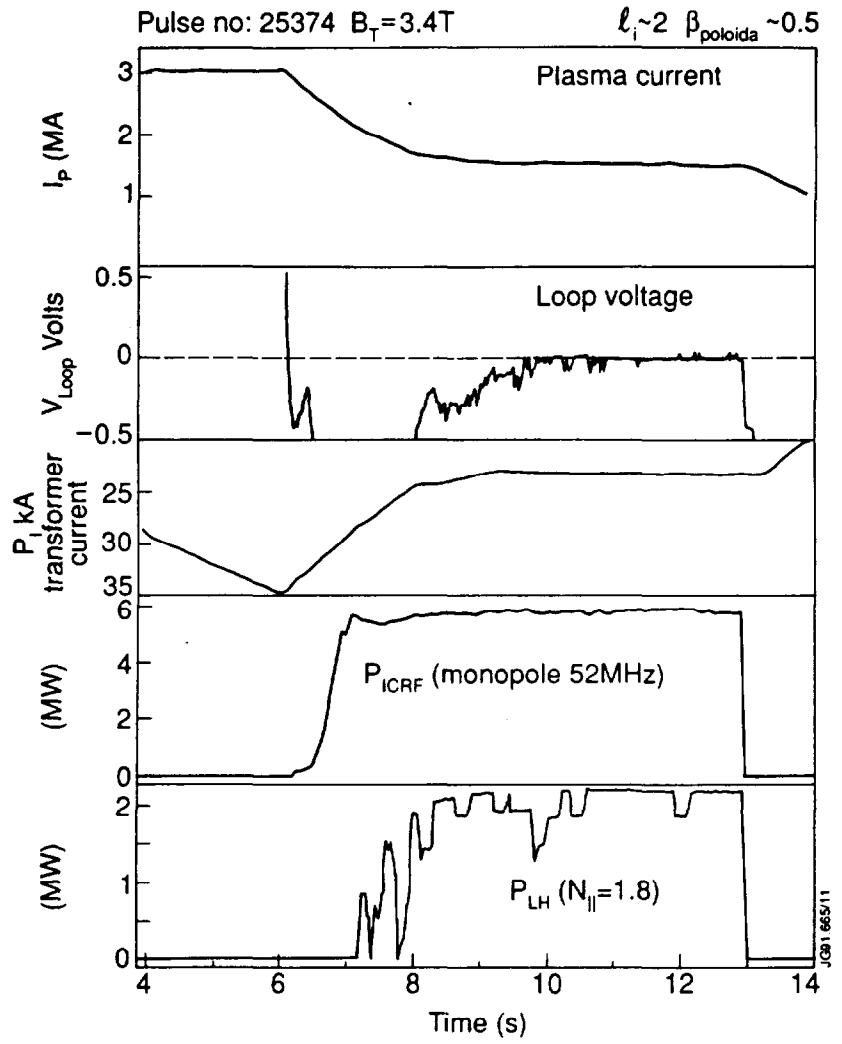

Fig 13: Full current drive with combined LHCD and ICRF at 1.5 MA.

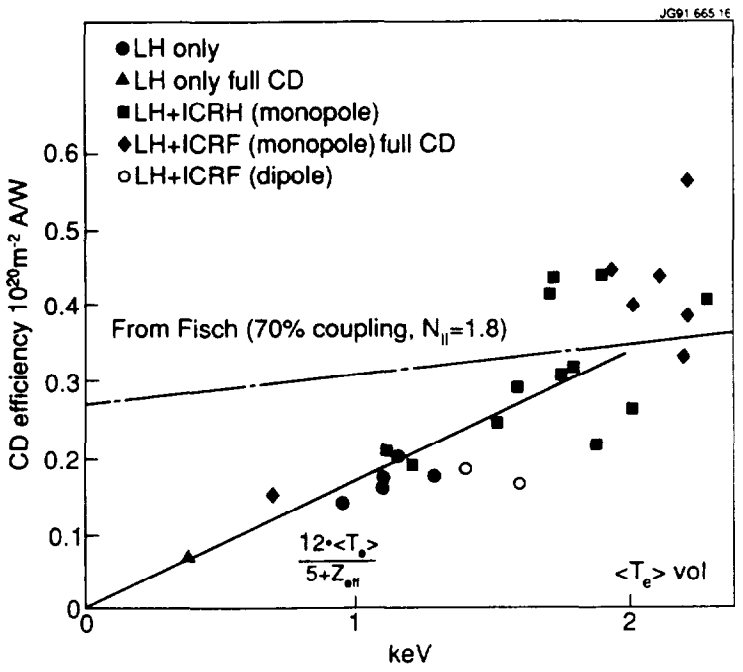

Fig 14: Current drive efficiency versus volume averaged electron temperature assumming all the non-inductive current drive being produced by LHCD and by the bootstrap current.

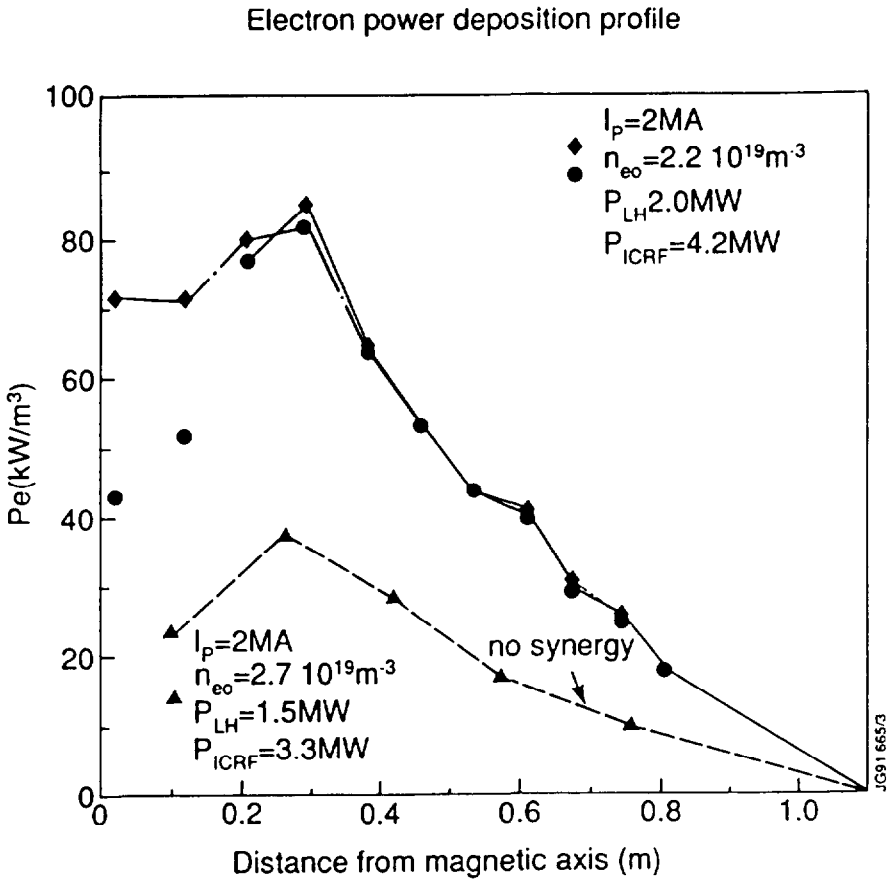

Fig 15: Electron power deposition profile(from ECE measurements). Integrated power is 1.1 MW for the pulse without synergy and 2.3 MW for the pulse with synergy.

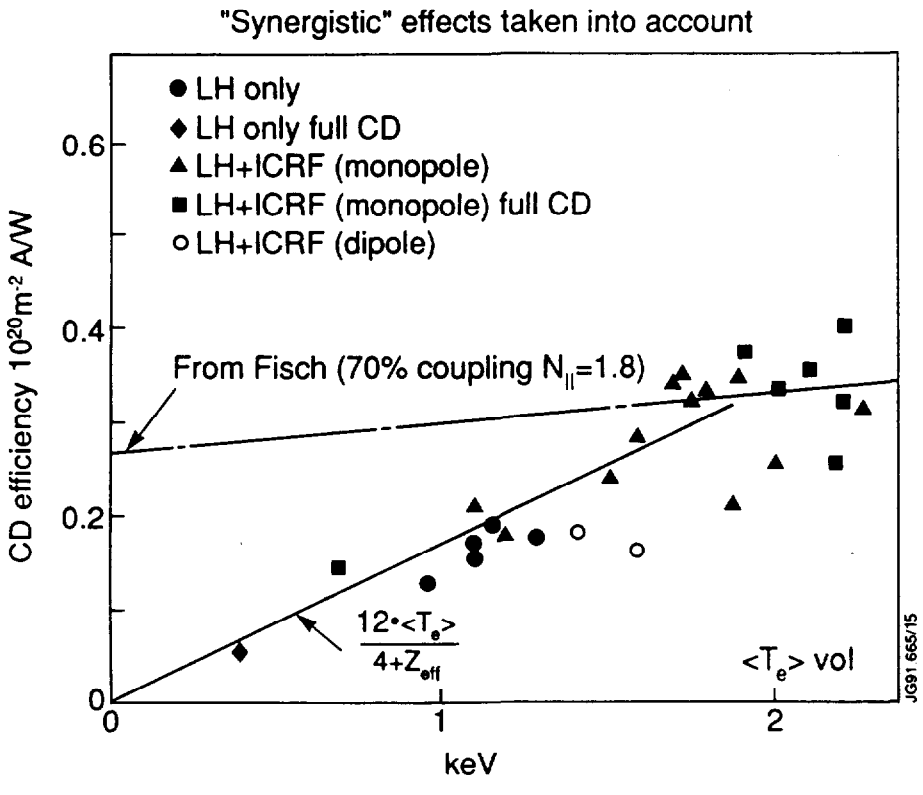

Fig 16: Current drive efficiency versus volume averaged electron temperature assuming taking into account synergistic effects.

Appendix I

THE JET TEAM

JET Joint Undertaking, Abingdon, Oxon, OX14 3EA, U.K.

J.M. Adams[1], H. Altmann, A. Andersen[14], P. Andrew[18], M. Angelone[29], S.A. Arshad, W. Bailey, P. Ballantyne, B. Balet, P. Barabaschi, R. Barnsley[2], M. Baronian, D.V. Bartlett, A.C. Bell, I. Benfatto[5], G. Benali, H. Bergsaker[11], P. Bertoldi, E. Bertolini, V. Bhatnagar, A.J. Bickley, H. Bindslev[14], T. Bonicelli, S.J. Booth, G. Bosia, M. Botman, D. Boucher, P. Boucquey, P. Breger, H. Brelen, H. Brinkschulte, T. Brown, M. Brusati, T. Budd, M. Bures, T. Businaro, P. Butcher, H. Buttgereit, C. Caldwell-Nichols, D.J. Campbell, P. Card, G. Celentano, C.D. Challis, A.V.Chankin[23], D. Chiron, J. Christiansen, C. Christodoulopoulos, P. Chuilon, R. Claesen, S. Clement, E. Clipsham, J.P. Coad, M. Comiskey[4], S. Conroy, M. Cooke, S. Cooper, J.G. Cordey, W. Core, G. Corrigan, S. Corti, A.E. Costley, G. Cottrell, M. Cox[7], P. Cripwell, H. de Blank[15], H. de Esch, L. de Kock, E. Deksnis, G.B. Denne-Hinnov, G. Deschamps, K.J. Dietz, S.L. Dmitrenko, J. Dobbing, N. Dolgetta, S.E. Dorling, P.G. Doyle, D.F. Düchs, H. Duquenoy, A. Edwards, J. Ehrenberg, A. Ekedahl, T. Elevant[11], S.K. Erents[7], L.G. Eriksson, H. Fajemirokun[12], H. Falter, D. Flory, J. Freiling[15], C. Froger, P. Froissard, K. Fullard, M. Gadeberg, A. Galetsas, D. Gambier, M. Garribba, P. Gaze, R. Giannella, A. Gibson, R.D. Gill, A. Girard, A. Gondhalekar, C. Gormezano, N.A. Gottardi, C. Gowers, B.J. Green, R. Haange, G Haas, A. Haigh, G. Hammett[6], C.J. Hancock, P.J. Harbour, N.C. Hawkes[7], P. Haynes[7], J.L. Hemmerich, T. Hender[7], F.B. Herzog, R.F. Herzog, J. Hoekzema, J. How, M. Huart, L Hughes, T.P. Hughes[4], M. Hugon, M. Huguet, A. Hwang[7], B. Ingram, M. Irving, J. Jacquinot, H. Jaeckel, J.F. Jaeger, G. Janeschitz[13], S. Jankowicz[22], O.N. Jarvis, F. Jensen, E.M. Jones, L.P.D.F. Jones, T.T.C. Jones, J-F. Junger, E. Junique, A. Kaye, B.E. Keen, M. Keilhacker, G.J. Kelly, W. Kerner, R. Konig, A. Konstantellos, M. Kovanen[20], G. Kramer[15], P. Kupschus, R. Lässer, J.R. Last, B. Laundy, L. Lauro-Taroni, K. Lawson[7], M. Lennholm, A. Loarte, R. Lobel, P. Lomas, M. Loughlin, C. Lowry, B. Macklin, G. Maddison[7], G. Magyar, W. Mandl[13], V. Marchese, F. Marcus, J. Mart, E. Martin, R. Martin-Solis[8], P. Massmann, G. McCracken[7], P. Meriguet, P. Miele, S.F. Mills, P. Millward, R. Mohanti[17], P.L. Mondino, A. Montvai[3], S. Moriyama[28], P. Morgan, H. Morsi, G. Murphy, M. Mynarends, R. Myrnäs[16], C. Nardone, F. Nave[21], G. Newbert, M. Newman, P. Nielsen, P. Noll, W. Obert, D. O'Brien, J. O'Rourke, R. Ostrom, M. Ottaviani, M. Pain, F. Paoletti, S. Papastergiou, D. Pasini, A. Peacock, N. Peacock[7], D. Pearson[12], R. Pepe de Silva, G. Perinic, C. Perry, M. Pick, R. Pitts[7], J. Plancoulaine, J-P. Poffé, F. Porcelli, L. Porte[19], R. Prentice, S. Puppin, S. Putvinsko[23], G. Radford[9], T. Raimondi, M.C. Ramos de Andrade, P-H. Rebut, R. Reichle, E. Righi, F. Rimini, D. Robinson[7], A. Rolfe, R.T. Ross, L. Rossi, R. Russ, P. Rutter, H.C. Sack, G. Sadler, G. Saibene, J.L. Salanave, G. Sanazzaro, A. Santagiustina, R. Sartori, C. Sborchia, P. Schild, M. Schmid, G. Schmidt[6], B. Schunke, S.M. Scott, A. Sibley, R. Simonini, A.C.C. Sips, P. Smeulders, R. Stankiewicz[27], M. Stamp, P. Stangeby[18], D.F. Start, C.A. Steed, D. Stork, P.E. Stott, T.E. Stringer, P. Stubberfield, D. Summers, H. Summers[19], L. Svensson, J.A. Tagle[21], A. Tanga, A. Taroni, A. Tesini, P.R. Thomas, E. Thompson, K. Thomsen, J.M. Todd, P. Trevalion, B. Tubbing, F. Tibone, E. Usselmann, H. van der Beken, G. Vlases, M. von Hellermann, T. Wade, C. Walker, R. Walton[6], D. Ward, M.L. Watkins, M.J. Watson, S. Weber[10], J. Wesson, T.J. Wijnands, J. Wilks, D. Wilson, T. Winkel, R. Wolf, B. Wolle[24], D. Wong, C. Woodward, Y. Wu[25], M. Wykes, I.D. Young, L. Zannelli, Y. Zhu[26], W. Zwingmann.

PERMANENT ADDRESSES

1. UKAEA, Harwell, Didcot, Oxon, UK.
2. University of Leicester, Leicester, UK.
3. Central Research Institute for Physics, Academy of Sciences, Budapest, Hungary.
4. University of Essex, Colchester, UK.
5. ENEA-CNR, Padova, Italy.
6. Princeton Plasma Physics Laboratory, New Jersey, USA.
7. UKAEA Culham Laboratory, Abingdon, Oxon, UK.
8. Universidad Complutense de Madrid, Spain.
9. Institute of Mathematics, University of Oxford, UK.
10. Freien Universität, Berlin, F.R.G.
11. Swedish Energy Research Commission, S-10072 Stockholm, Sweden.
12. Imperial College of Science and Technology, University of London, UK.
13. Max Planck Institut für Plasmaphysik, Garching bei München, FRG.
14. Risø National Laboratory, Denmark.
15. FOM Instituut voor Plasmafysica, 3430 Be Nieuwegein, The Netherlands.
16. University of Lund, Sweden.
17. North Carolina State University, Raleigh, NC, USA
18. Institute for Aerospace Studies, University of Toronto, Downsview, Ontario, Canada.
19. University of Strathclyde, 107 Rottenrow, Glasgow, UK.
20. Nuclear Engineering Laboratory, Lapeenranta University, Finland.
21. CIEMAT, Madrid, Spain.
22. Institute for Nuclear Studies, Otwock-Swierk, Poland.
23. Kurchatov Institute of Atomic Energy, Moscow, USSR
24. University of Heidelberg, Heidelberg, FRG.
25. Institute for Mechanics, Academia Sinica, Beijing, P.R. China.
26. Southwestern University of Physics, Leshan, P.R. China.
27. RCC Cyfronet, Otwock Swierk, Poland.
28. JAERI, Naka Fusion Research Establishment, Ibaraki, Japan.
29. ENEA, Frascati, Italy.

At 1st June 1991